Contents lists available at ScienceDirect

Arabian Journal of Chemistry

journal homepage: www.ksu.edu.sa

Original article

Inhibitory effects of platinum nanoparticles coated with polyethylene glycol and conjugated with Rutin on the MCF-7 breast cancer cell line

Yue Li [a,1], Jianming Guo [b,1], Xue Gong [b], Huanyu Zhang [b], Keru Ma [b], Yuan Sui [b], Baihui Chen [b], Yubo Du [b], Tianyu Chen [b], Dongxu Yang [b], Dalin Li [b,*]

[a] Department of Medical Oncology, Harbin Medical University Cancer Hospital, Harbin 150086, China
[b] Department of Breast Surgery, Harbin Medical University Cancer Hospital, Harbin 150086, China

ARTICLE INFO

Keywords:
Apoptosis
Breast cancer
Platinum nanoparticles
Rutin

ABSTRACT

The objective of this work is to characterize the anticancer mechanism of platinum nanoparticles coated with polyethylene glycol and conjugated with Rutin (Rutin-PEG-PtNPs) in a breast cancer cell line. PtNPs were synthesized using *Dendrobium officinale* extract, coated with PEG, conjugated with Rutin, and characterized by the FT-IR, XRD, DLS, and TEM. The viability of the breast cancer cells (MCF-7) and normal breast cells (MCF-10A) after treatment with PEG-PtNPs and Rutin-PEG-PtNPs was studied by the MTT assay. Superoxide dismutase (SOD) and catalase (CAT) activity, MDA level, and LDH leakage in the PEG-PtNPs and Rutin-PEG-PtNPs were measured. The expression of the *p53*, *Bax*, *Bcl-2*, and *caspase −8,* and *−9* genes, as well as the NF-κB and IL-6 levels in the Rutin-PEG-PtNPs treated cells, were investigated by qPCR and ELISA assays. Results demonstrated that the NPs were in a size range of 30 to 60 nm. The Rutin-PEG-PtNPs showed greater cytotoxic effects on breast cancer cells (IC_{50}: 45.5 μg/mL) than normal breast cells (IC_{50}: 69.4 μg/mL). The expression of the *p53*, *Bax*, *caspase-8,* and *−9* was upregulated by 1.96, 1.84, 1.31, and 2.79 folds, while the expression of the *Bcl-2* was reduced in Rutin-PEG-PtNP-treated cells. The activity of the SOD and CAT decreased, while the LDH leakage and MDA levels increased after treating the cells with Rutin-PEG-PtNPs. Also, the NF-κB and IL-6 levels in the cell cultures treated with Rutin-PEG-PtNPs were reduced by 22.6 and 17.0 %, respectively. Rutin-PEG-Pt indicated promising inhibitory potential against MCF-7 cells.

1. Introduction

The occurrence of metastatic and multi-drug resistant types has raised a serious challenge in the treatment of breast cancer, so many cases of the disease are not responsive to chemotherapy drugs. With 0.7 million deaths per year, breast cancer is currently known as the most important and deadly cancer in the female population, worldwide (Sung et al., 2021).

With the emergence of nanotechnology, the use of nanoproducts in various fields is increasing. Nowadays, various NPs are synthesized and evaluated for disease diagnosis and treatment. Due to their high stability, appropriate reactivity, relatively easy and cheap production, and promising antimicrobial and anticancer properties, metal NPs have received much attention to be employed in biomedical applications (Khursheed et al., 2022). However, the clinical use of many metal NPs has been limited due to their low biocompatibility and relatively high toxicity. Coating metal NPs with biocompatible materials can be a suitable approach to reduce toxicity and improve the safety of metal NPs (Sur et al., 2019). Also, such an approach provides the possibility of conjugating various compounds to metal NPs to improve their efficacy and develop their application.

After the introduction of Pt-containing drugs, including cisplatin and oxaliplatin in anticancer chemotherapy, the use of Pt in biomedical fields has received increasing attention. Due to remarkable catalytic activity, ability to generate reactive oxygen species (ROS), stability, and relatively good biocompatibility, PtNPs can be considered a candidate to be used against various cancer cells (Pedone et al., 2017). However, systemic toxicity of Pt-based anticancer agents is still a major challenging problem in the clinical application of such drugs. Several modification approaches, such as coating with biocompatible compounds and linking to drug delivery carriers, have been proposed to reduce their toxicity (Zhang et al., 2022). Surface decoration of metal

* Corresponding author at: No.150 Haping Road, Nangang District, Harbin 150086, Heilongjiang Province, China.
E-mail address: lidalin1975@163.com (D. Li).
[1] Contribute equally to this study.

https://doi.org/10.1016/j.arabjc.2023.105567
Received 28 October 2023; Accepted 13 December 2023
Available online 16 December 2023

NPs with biocompatible polymers such as PEG, chitosan, xanthan, etc. has been introduced to improve stability and biocompatibility of NPs (Muddineti et al., 2015). Furthermore, it can facilitate the conjugating of different functionalizing agents such as therapeutic ligands, drugs, peptides, and surfactants to NPs in order to improve their anticancer efficacy (Pawar et al., 2021). Several studies reported that PtNPs exhibit synergistic anticancer effects when combined with bioactive compounds and drugs. It has been reported that PtNPs, in combination with Doxorubicin, can induce DNA damage and exert cytotoxic effects on cancer cells through induction of oxidative stress (Gurunathan et al., 2019). Furthermore, phytic acid-capped PtNPs showed improved anticancer effects on cancer cells (Zhou et al., 2019).

The biological production of metal NPs has several advantages over chemical synthesis methods. In this method, NPs are synthesized using plant, algal, or bacterial extracts, which reduces the possibility of forming toxic compounds. In addition, the synthesized NPs show better biocompatibility compared to the chemically synthesized types (Zhao et al., 2021). It has been reported that biogenic synthesized PtNPs have very low toxic effects on normal human cells, and therefore, their use in biomedical fields can be associated with fewer challenges (Aygun et al., 2020).

Rutin is an herbal flavonoid that is typically found in a variety of fruits, vegetables, and plant-derived compounds. The pharmacological properties of Rutin, including anticancer, antimicrobial, anti-inflammatory, and antioxidation effects, have been extensively described in the literature (Imani et al., 2021). A large number of *in-vitro* and *in-vivo* studies reported remarkable anticancer activity of Rutin. The antiproliferative mechanisms of Rutin include the generation of oxidative stress, activation of caspases, ER stress, and cell cycle arrest, which finally lead to cell apoptosis (Imani et al., 2021). Considering the promising anticancer properties of Rutin and PtNPs, in this study, PtNPs were synthesized using the *Dendrobium officinale* whole plant extract, and the apoptogenic properties of PtNPs coated with PEG and conjugated with Rutin (Rutin-PEG-PtNPs) in the MCF-7 breast cancer cell line was investigated. The effect of treatment with Rutin-PEG-PtNPs on viability, oxidative stress biomarkers, LDH leakage, and interleukine level was characterized. Also, the expression of some pro- and anti-apoptotic genes in control and treated cells was investigated. To our knowledge, the anticancer efficacy and mechanism of PtNPs conjugated with Rutin have not been investigated yet. This study introduces Rutin-PEG-Pt as a promising inhibitory candidate of the MCF-7 breast cancer cells for the first time.

2. Materials and methods

2.1. Preparation of Dendrobium officinale extract

D. officinale whole plant powder was purchased from the local market. To prepare the extract, 100 g of *D. officinale* powder was heated in one liter of distilled water at 90 ℃ for 60 min. Then, the extract was centrifuged for 10 min, the supernatant was filtered, and stored at 4 ℃.

2.2. Green synthesis of platinum nanoparticles

Green synthesis of PtNPs was performed according to the method described by Aygun et al., with minor modifications (Aygun et al., 2020). In brief, 20 mL of *D. officinale* extract was added to 80 mL of 1 mM aqueous $H_2PtCl_6{\cdot}6H_2O$ (Sigma-Aldrich). The mixture was transferred to a 100 °C water bath for 60 min. Then, the temperature was reduced to 75 ℃ and the mixture was shaken for 24 h. After the formation of black particles, PtNPs were purified and washed by repeated centrifugation at 12,000 rpm for 15 min in ethanol and distilled water to remove the impurities. Then, the particles were dried at 60 ℃ and subjected to characterization studies.

2.3. Coating with PEG

PEG-coated PtNPs were prepared according to the method described by Phadatare et al. (2012), with minor modifications. To prepare PEG-coated PtNPs, 8 mL of 1 mM concentration of PEG (Sigma-Aldrich) in distilled water was added to 20 mL of 1.25 mg/mL suspension of PtNPs. The solution was sonicated for 2 h at room temperature and then, was shaken for 24 h at 100 rpm. Then, the particles were harvested by centrifugation, washed several times with ethanol, and dried under a vacuum.

2.4. Conjugation with Rutin

At first, 5 mL of a stock solution of Rutin (8 mg/mL) (Sigma-Aldrich) was prepared in DMSO. Then, PEG-coated PtNPs were suspended in 30 mL of DMSO and Rutin. The mixture was shaken at 100 rpm, overnight. Next, the pH of the mixture was adjusted to 8.5 using 1 M NaOH solution. Finally, Rutin-PEG-PtNPs were collected, washed with ethanol and distilled water, and dried.

2.5. Characterization of particles

Synthesis of NPs was confirmed by FT-IR, XRD, and TEM imaging. FT-IR spectrum was determined using a JASCO FT-IR 4100 instrument (Japan). The XRD assay was used to study the crystal structure of the NPs using a Drawell XRD diffractometer (DW-XRD-2700A) with CuK radiation, 40 kV, k = 1.54056 Å). Also, TEM (JEOL 2100, Japan) microscopy was used to examine the size of the particles. Furthermore, the hydrodynamic size of the particles was measured by a DLS analysis.

2.6. Cell culture

Two breast cell lines, including the MCF-7 breast cancer as well as normal breast cells (MCF-10A), were included in this work. The cell lines were obtained from Cell Bank of the Chinese Academy of Sciences (Shanghai, China) and cultured in Dulbecco's modified eagle's medium (DMEM) supplemented with streptomycin (100 units/mL), penicillin (100 units/mL), and fetal bovine serum (10 % v/v), under carbon dioxide (5 %) and at 37 ℃ (Biobase BJPX-C80 incubator, China).

2.7. Cell viability assay

Cell viability was evaluated using the MTT cell viability assay. At first, the monolayer of the cells was grown in 96-well plates. A stock solution (3200 μg/mL) of the NPs was prepared in PBS, and then, breast cancer and non-cancerous cells were treated with PEG-PtNPs and Rutin-PEG-PtNPs at final concentrations ranging from 5 to 320 μg/mL. Untreated cells were considered negative control, and cisplatin was used as a standard anticancer drug. The plates were incubated for 24 h at 37 ℃. Next, 10 μL of MTT solution (Sigma-Aldrich) was added to the wells and incubated for 5 h, then the medium was aspirated and 150 μL of DMSO (Sigma-Aldrich) was added to dissolve the formed formazan salt. The optical density at 570 nm was measured using a plate reader (Biobase BK-EL10C, China), and cell viability was quantified based on the color intensity of the formazan solution and 25 %, 50 %, and 75 % inhibitory concentrations of the NPs (IC_{25}, IC_{50}, and IC_{75}) were calculated.

2.8. Characterization of exposure time

The effect of exposure time with PEG-PtNPs and Rutin-/PEG-PtNPs on the survival of breast cancer and normal cells was evaluated. At first, cell monolayers were grown in cell culture plates and then, treated with PEG-PtNPs and Rutin-PEG-PtNPs at their IC_{25}, IC_{50}, and IC_{75} concentrations. The plates were incubated at 37 ℃, and the cell viability was measured at 3-hour intervals using the MTT assay, as described above.

2.9. MDA level

The level of malondialdehyde, which is considered an oxidative stress biomarker, was measured in the control and treated cells using the Sigma-Aldrich commercial kit (Cat no.MAK085), according to the instructions. In brief, the MCF-7 cells were treated with PEG-PtNPs and Rutin-PEG-PtNPs at IC_{50} and IC_{75} concentrations. The cells were incubated for 24 h, and next, the cells were harvested and 300 μL of lysis buffer was added to the cells. The vials were centrifuged for 10 min at 13,000 × g and 250 μL of the supernatant and 650 μL of the thiobarbituric acid (TBA) solution were transferred to a new vial and incubated at 95 °C for 5 min. The mixture was centrifuged (14000 g) for 5 min. Finally, the optical absorption at 532 nm was measured, and the quantity of MDA was calculated using a standard curve.

2.10. The activity of antioxidant enzymes

The MCF-7 cells were treated with PEG-PtNPs and Rutin-PEG-PtNPs for 24 h and then, subjected to quantification of the activity of the superoxide dismutase (SOD) (Sigma-Aldrich, 19160) and catalase (CAT) (Sigma-Aldrich, MAK381) according to the manufacturer's instruction. To determine SOD activity, 20 μL of cell supernatant sample was added to 200 μL of working solution, and then 20 μL of enzyme solution was added. The plate was incubated at 37 ℃ for 20 min, and then, the absorbance at 450 nm was recorded. To quantify CAT activity, 10 μL of cell supernatant to a well, and the volume was adjusted to 78 μL using CAT assay buffer. Then, 12 μL of 1 mM H_2O_2 was added, incubated for 40 min at room temperature, and then 10 μL of stop solution was added. Finally, absorbance at 570 nm, which corresponds to CAT activity, was recorded. The assay was performed in three replicates and untreated cells were considered as the control group. The assay was performed in three replicates and untreated cells were considered as the control group.

2.11. Lactate dehydrogenase (LDH) leakage assay

Measuring lactate dehydrogenase (LDH) was carried out on the cells treated with PEG-PtNPs and Rutin-PEG-PtNPs as well as the control cells. The MCF-7 cells were treated with the NPs at IC_{50} and IC_{75} concentrations for 24 h, and then subjected to an LDH leakage assay using the method described by Alarifi et al. (2014). In Brief, 100 μL of culture medium was added to 3 mL of assay solution containing pyruvic acid (2.2 mg/mL), NADH (2.5 mg/mL), and PBS. The tube was incubated for 3 min and the LDH level was measured by the decrease in absorbance at 340 nm (Biobase BK-V1200 spectrophotometer). The assay was performed in three replicates and untreated cells were considered as the control group.

2.12. Quantitative real-time PCR (qPCR)

The expression of several genes related to the regulation of apoptosis pathways was characterized. The studied genes include *caspase −8 and −9*, *Bcl-2*, *Bax*, and *p53*. At first, MCF-7 cells were treated with PEG-PtNPs and Rutin-PEG-PtNPs at their IC_{50} concentration for 24 h at 37 ℃. Then, the cells were collected and washed several times with PBS buffer, and their RNA content was extracted by a TIANGEN RNA extraction kit (Cat. no.4992732). After quantification of RNA, gene amplification was performed by a TIANGEN FastKing SYBR Green One-Step qPCR Kit (Cat no.4993103) and using the primers that were presented in Table 1. Gene amplification was performed in three replicates. The *GAPDH* gene was also considered an internal control gene. Amplification of the gene fragments was performed in a final volume of 12.5 μL and using a pre-defined thermal program in an ABI PRISM 7300 (Applied Biosystem, USA) instrument. Gene expression, relative to the control gene, was quantified using the $2^{-\Delta\Delta ct}$ method (Livak and Schmittgen, 2001).

2.13. NF-κB and IL-6 level

To determine the NF-κB and IL-6 levels, the MCF-7 cells were treated with PEG-PtNPs and Rutin-PEG-PtNPs at their IC_{50} concentration for 24 h. Then, the cells were harvested, homogenized in PBS buffer, and centrifuged at 5000 g for 8 min. The supernatant was collected and was used to quantify the NF-κB and IL-6 levels using the human NF-κB (MyBioresource, cat no: MBS260716) and human Interleukin 6 (IL-6) (SinoBiological, Cat. No. KIT10395A) ELISA Kits, according to the instructions. To quantify the NF-κB level, 100 μL of cell supernatant samples were added to the wells and incubated at 37 ℃ for 90 min. Then, 100 μL of antibody solution was added and the plate was further incubated for 60 min. Next, 100 μL of Enzyme conjugate (37 ℃/30 min), and then 100 μL of color reagent was added and OD450 was measured and compared with standards. To Quantify the IL-6 level, 100 μL of cell supernatant samples were added to the wells, incubated for 2 h at room temperature, and then 100 μL of detection antibody solution was added and incubated for 60 min at room temperature. After aspirating the content, 100 μL of the substrate solution (20 min/ room temperature) and then, stop solution was added. Finally, absorbance at 450 nm was recorded. The assay was performed in three replicates.

2.14. Statistical analysis

The results were analyzed with one-way analysis of variance using SPSS software, and the $p < 0.05$ was considered statistically significant. Microsoft Excel 2010 was used for the graphical representation.

3. Results

3.1. Characterization of the synthesized particles

FT-IR analysis was used to characterize the functional groups of the synthesized particles. Considering the spectrogram of PtNPs, two intense bands at 987 and 1636 cm^{-1} are assigned to the C-H bonds. A medium band at about 1440 cm^{-1} can be assigned to the C = C bond. The band at 3465 cm^{-1} is related to O-H stretching. According to the FT-IR spectrogram of Rutin-PEG-PtNP, five additional bands at 1041, 1462, 1649, 2971, and 3497 cm^{-1} could be observed that may be related to the C = C stretching, C-C bond, C = O stretching vibration, C-H stretching, and O-H stretching, respectively. The bands at 465–680 cm^{-1} may be related to metal–carbon bonds. Evaluating the bands associated with Rutin, a strong O-H stretching that is expected at 3200–3600 cm^{-1} was observed

Table 1
Sequences of primers used for qPCR.

Gene	Forward primer	Reverse primer	Reference
p53	5́-CCCAGCCAAAGAAGAAACCA-3́	5́-TTCCAAGGCCTCATTCAGCT-3́	Ahamed et al., 2011
Bcl-2	5́- TCGCCCTGTGGATGACTGAG-3́	5́- CAGAGTCTTCAGAAGACAGCCAGGA −3́	Banafa et al., 2013
Bax	5́-GGGCTGGACATTGGACTTCC-3́	5́-AGATGGTGAGTGAGGCGGTG-3́	Banafa et al., 2013
caspase-9	5́-CCAGAGATTCGCAAACCAGAGG-3́	5́-GAGCACCGACATCACCAAATCC-3́	Ahamed et al., 2011
caspase-8	5́- ACCTTGTGTCTGAGCTGGTCT −3́	5́- GCCCACTGATATTCCTCAGGC −3́	Farasat et al., 2020
GAPDH	5́-GTGGAAGGACTCATGACCACAG-3́	5́-CTGGTGCTCAGTGTAGCCCAG-3́	Banafa et al., 2013

at 3497 cm^{-1}. Furthermore, a C-H stretching (2850–2950 cm^{-1}) was determined at 2927 cm^{-1}. Also, a weak C-C band (expected at 1400–1600 cm^{-1}) was observed at 1462 cm^{-1}. The FT-IR spectrum of rutin was reported by Ramaswamy et al. (2017) and Kızılbey (2019), that are in agreement with our results. Moreover, most of the peaks related to PtNPs could be observed in the FT-IR spectrogram of Rutin-PEG-PtNPs, with minor shifting. A similar FT-IR pattern for Pt and PEG-PtNPs has been reported by Mukherjee et al., (2020). Overall, comparing the FT-IR spectrograms indicates coating of the PtNPs with PEG and conjugating with Rutin (Fig. 1).

The XRD pattern of the NPs indicates distinct reflections at 2θ of 37.2°, 44.2°, 67.9°, and 78.1° that are related to the face-centered cubic Pt structure (JCPDS Card No. 04–0802) (Zheng et al., 2013). The face-centered cubic crystallite size of PtNPs has been indicated by Mukherjee et al., (2020), which is in agreement with this work. A similar XRD pattern was also reported by Aygun et al., (2020), who synthesized PtNPs using *Nigella sativa L.* extract. Also, the peaks at 2θ of 20.1–29.2° can be associated with the presence of Rutin and PEG molecules (Fig. 2) (Saha and Mishra, 2020).

According to electron microscopy imaging, a medium agglomeration state of the particles was observed. TEM microscopy showed that the majority of particles are spherical (Fig. 3). However, due to the coating of the particles with PEG, some particles tend to be assembled into a chain-like structure upon electrostatic interactions. This can indirectly support the surface coating of PtNPs. A similar characteristic was reported previously (Mukherjee et al., 2020). TEM images also revealed the synthesized NPs had sizes in the range of 30 to 60 nm (Fig. 3). Furthermore, the size of the Rutin-PEG-PtNPs deduced by the DLS study was 122 nm (Fig. 4). The larger DLS size than TEM ones seems to be associated with the hydration of the particles in the aqueous medium.

3.2. Cell viability

According to the cell viability assay, PEG-Pt and Rutin-PEG-PtNPs had remarkable cytotoxic effects on breast cancer cells. According to the results, the NPs had concentration-dependent cytotoxicity which significantly reduced viability of MCF-7 cells. Comparing the viability of the cancer cells treated with PEG-PtNPs and Rutin-PEG-PtNPs showed that conjugating with Rutin, significantly enhanced the cytotoxic property of the NPs. The IC_{25}, IC_{50}, and IC_{75} of the PEG-PtNPs for MCF-7 cells were 21.6, 70.1, and 212.9 μg/mL, respectively, while these values for the Rutin-PEG-PtNPs were 16.2, 45.5, and 128.0 μg/mL. Similarly, the NPs showed a cytotoxic effect on normal breast cells, however, they were less toxic for the normal cells than breast cancer cells. The IC_{50} of PEG-Pt and Rutin-PEG-PtNPs for normal breast cells were 94.6 and 69.4 μg/mL, which suggests lower cytotoxicity of the NPs for the normal cells. In addition, cisplatin, which was used as a standard drug, showed the strongest cytotoxic effect on both cell lines with an IC_{50} of 16.8 and 16.3 μg/mL for breast cancer and normal breast cell lines, respectively (Table 2 and Fig. 5).

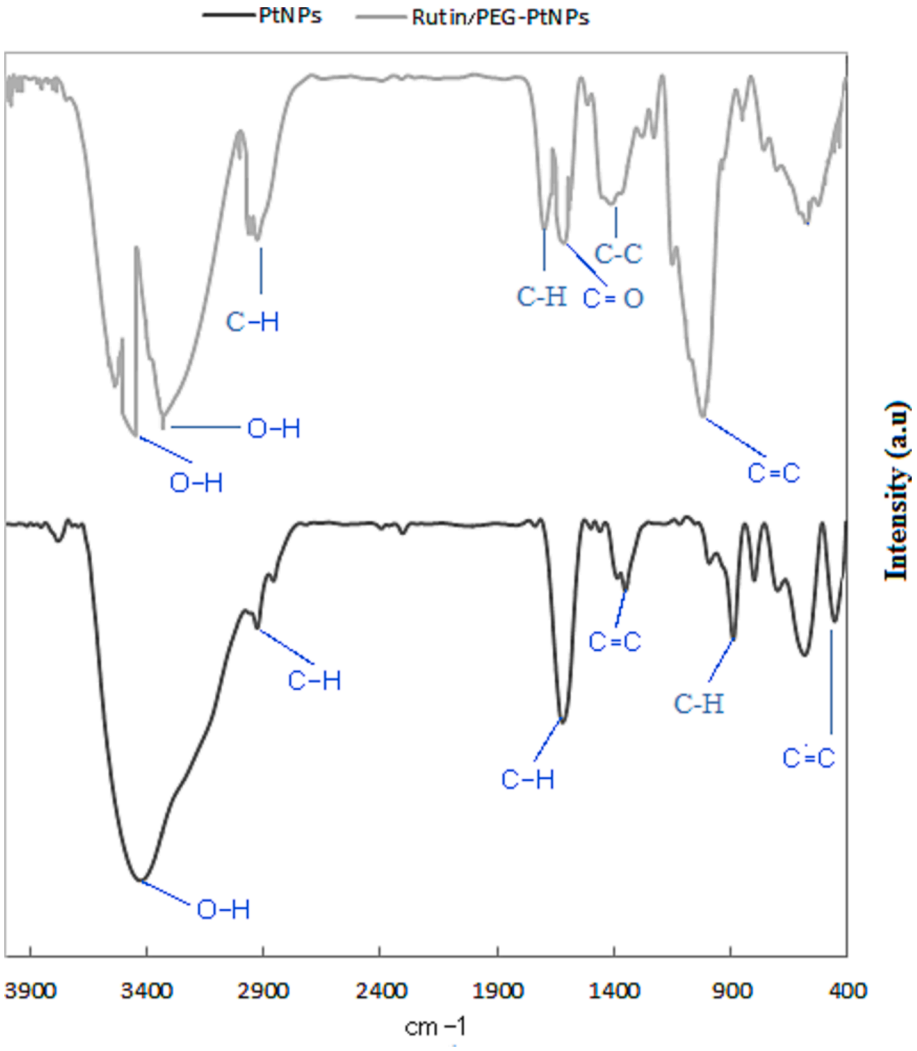

Fig. 1. FT-IR spectrum of PtNPs and Rutin-PEG-PtNPs.

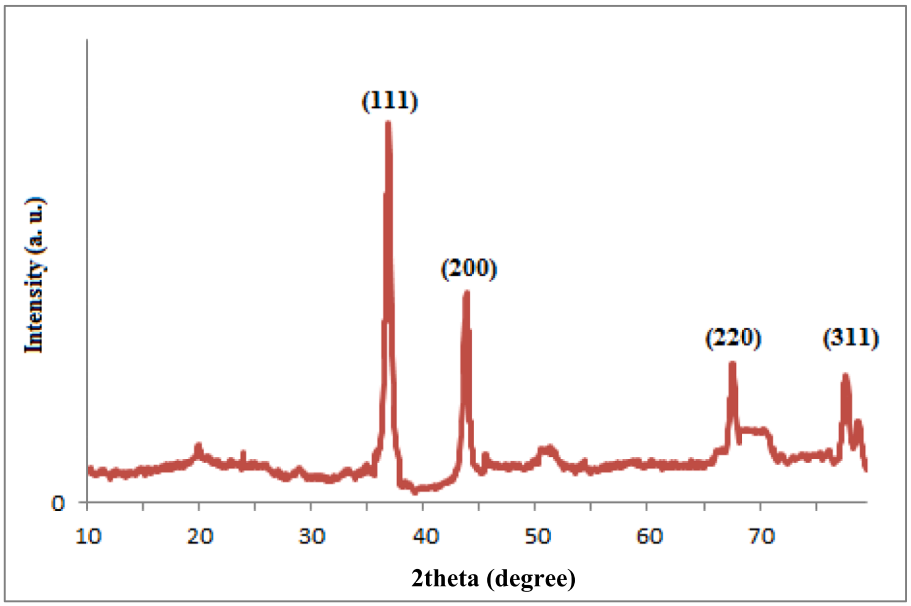

Fig. 2. XRD pattern of Rutin-PEG-PtNPs.

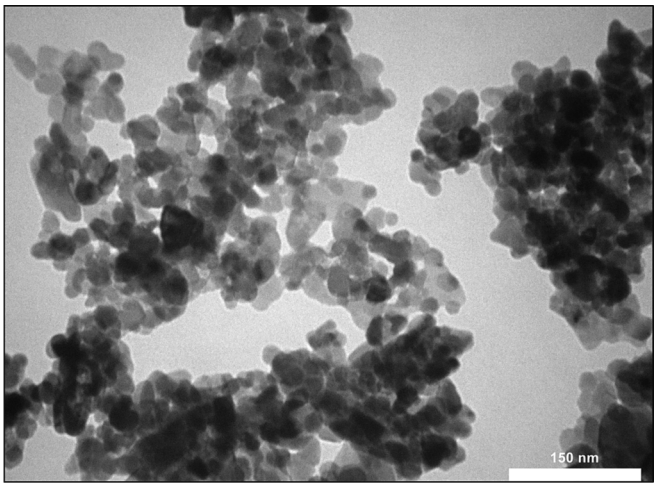

Fig. 3. TEM micrographs of Rutin-PEG-PtNPs.

3.3. Exposure time

The effect of exposure to different concentrations of the PEG-PtNPs and Rutin-PEG-PtNPs during 18 h on the viability of the MCF-7 and MCF-10A cell lines was characterized. According to the results, both NPs had dose-dependent and time-dependent toxic effects on the breast cancer and normal cell lines. Overall, Rutin-PEG-PtNPs were more toxic for both cell lines than PEG-PtNPs during different incubation periods. The viability of breast cancer cells at IC_{25}, IC_{50}, and IC_{75} concentrations of PEG-PtNPs reduced to 83.6, 56.8, and 29.9 %, respectively, while exposure to Rutin-PEG-PtNPs decreased cell viability to 78.0, 47.0, and 27.6 % at IC_{25}, IC_{50}, and IC_{75} concentrations. In addition, it was found that during 18 h of treatment and at IC_{25} and IC_{75} concentrations, there was a slight difference in the susceptibility of breast cancer and normal cells to Rutin-PEG-PtNPs. However, at IC_{50} concentration, Rutin-PEG-PtNPs showed more toxicity for the breast cancer cells than normal cells with viability percentages of 47.0 and 56.1 %, respectively. The results are demonstrated in Fig. 6.

3.4. Oxidative stress biomarkers

Assessment of the effect of the NPs on the SOD activity in MCF-7 cells showed that both NPs at their IC_{50} and IC_{75} concentrations reduced the activity of SOD. The enzyme activity in the cells treated with PEG-PtNPs and Rutin-PEG-PtNPs at their IC_{50} reduced by 24.2 % and 22.1 % respectively, while at their IC_{75} concentration, the enzyme activity reduced by 41.4 and 62.9 %, respectively (Fig. 7A).

The activity of CAT following treatment with PEG-PtNPs and Rutin-PEG-PtNPs decreased significantly. Exposure to PEG-PtNPs at their IC_{50} and IC_{75} concentrations reduced enzyme activity by 16.7 and 29.9 %, respectively, while Rutin-PEG-PtNPs decreased CAT activity by 32.7 and 70.2 % (Fig. 7B).

MDA level as a marker for lipid peroxidation was quantified in the control and NP-treated cancer cells. Treating MCF-7 cells with PEG-PtNPs and Rutin-PEG-PtNPs at IC_{50} concentration significantly increased the MDA level to 7.3 and 8.3 nmol/mg protein, respectively. Furthermore, at IC_{75} concentration, the MDA level significantly increased to 10.2 and 11.0 nmol/mg protein, while the MDA level in control cells was 4.1 nmol/mg protein (Fig. 7C).

3.5. LDH leakage

Membrane damage due to the exposure to NPs was examined by LDH leakage assay. According to the results, treating with Rutin-PEG-PtNPs led to more severe membrane damage compared with PEG-PtNPs. Treating with Rutin-PEG-PtNPs caused 141.9 % (IC_{50}) and 163.7 % (IC_{75}) of LDH release from MCF-7 cells, relative to control cells. In contrast, exposure to PEG-PtNPS at their IC_{50} and IC_{75} concentrations caused an increase of 117.2 and 129.0 % in the LDH leakage from breast cancer cells (Fig. 8).

3.6. qPCR assay

Characterizing the effect of treating breast cancer cells with PEG-PtNPs and Rutin-PEG-PtNPs revealed that the NPs can positively induce apoptotic genes. According to the results, PEG-PtNPs considerably induced the expression of the *Bax*, *p53*, *caspase-8*, and *caspase-9* genes. Treatment of the MCF-7 cells with Rutin-PEG-PtNPs significantly upregulated the expression of the *Bax* and *p53* genes. Moreover, the expression of the exprssion of the *Bcl-2* gene reduced to 0.79 folds.

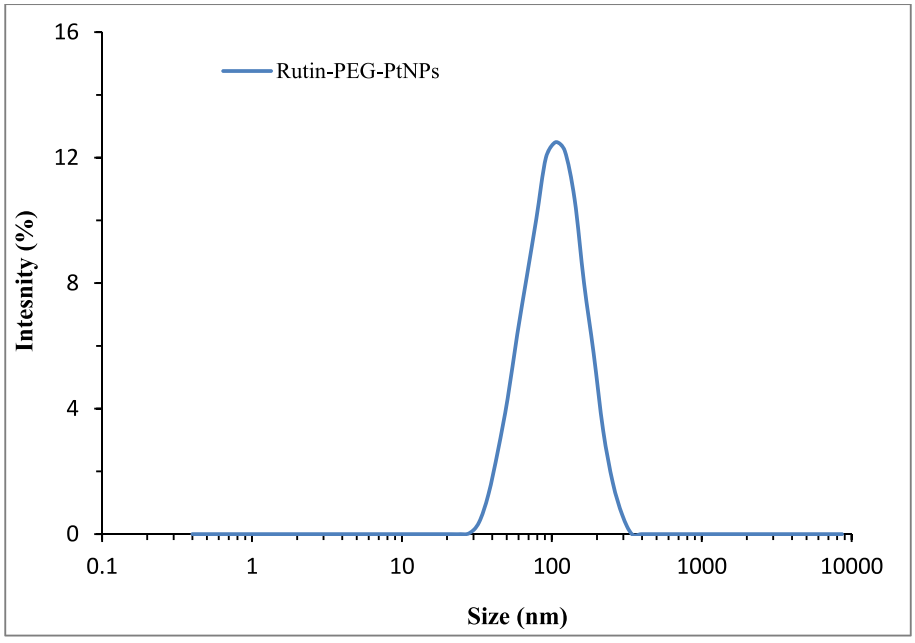

Fig. 4. Hydrodynamic size distribution of the Rutin-PEG-PtNPs.

Table 2
Inhibitory concentrations of cisplatin, PEG-PtNPs, and Rutin-PEG-PtNPs for studied cell lines.

	IC_{25} (μg/mL)		IC_{50} (μg/mL)		IC_{75} (μg/mL)	
	MCF-7	MCF-10A	MCF-7	MCF-10A	MCF-7	MCF-10A
Cisplatin	4.4	5.6	16.8	16.3	64.3	51.1
PEG-PtNPs	21.6	33.5	70.1	94.6	212.9	258.3
Rutin-PEG-PtNPs	16.2	15.1	45.5	69.4	128.0	256.1

Additonally, treating the cells with Rutin-PEG-PtNPs significantly increased the expression of the *caspase-9* gene by 2.79 folds, and the expression of the *caspase-8* was increased by 1.31 folds. The results are displayed in Fig. 9.

3.7. NF-κB and IL-6 level

Characterization of the effect of the PEG-PtNPs and Rutin-PEG-PtNPs on the level of proinflammatory cytokines was performed. As can be observed in Fig. 10a, treating with the Rutin-PEG-PtNPs NPs caused a significant reduction in the level of NF-κB (by 22.6 %), while PEG-PtNPs insignificantly reduced NF-κB level by 4.3 % in breast cancer cells. In contrast, treating with the PEG-PtNPs caused a slight increase in the IL-6 level in MCF-7 cells (9.2 %), while Rutin-PEG-PtNPs caused a reduction of 17 % in the IL-6 level. The results are displayed in Fig. 10b.

4. Discussion

Despite the widespread use of metal NPs in various applications, their use in medical applications faces many limitations due to high toxicity and unwanted side effects. Coating metal NPs using biocompatible compounds can be a solution to reduce the toxic effects of metal NPs and enable their wider application. Also, this method provides the possibility of adding effective medicinal compounds on the surface of NPs. Based on this approach, synthetic or natural compounds can be conjugated to metal NPs to increase their biological properties, including anticancer activity. Therefore, this study aims to investigate the anticancer effect and mechanism of PtNPs coated with PEG and

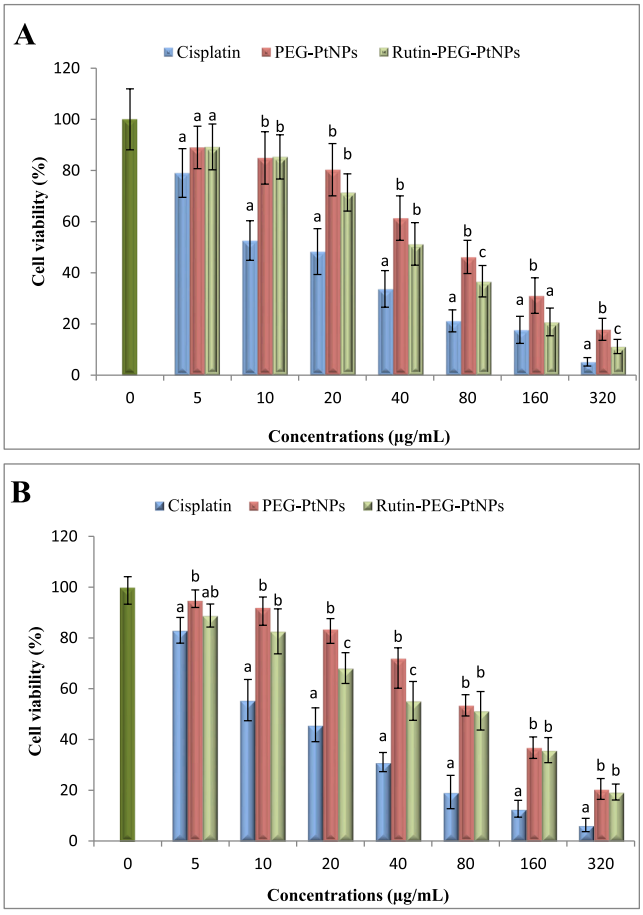

Fig. 5. Viability of the (A) MCF-7 and (B) MCF-10A cells after treatment with cisplatin, PEG-PtNPs, and Rutin-PEG-PtNPs. Different letters display significant differences ($p < 0.05$).

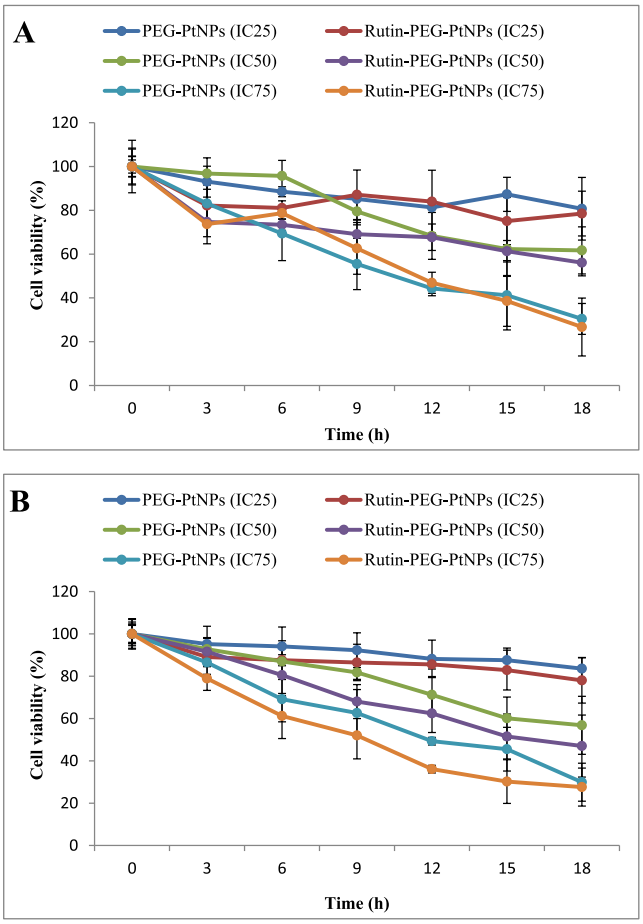

Fig. 6. Effect of exposure time on the viability of A) MCF-10A and B) MCF-7 cell lines. Rutin-PEG-PtNPs showed a time and concentration toxic effect on breast cancer cells which was stronger than normal cells at IC_{25} and IC_{50} concentrations.

loaded with Rutin on a breast cancer cell line. Examining the viability of breast cancer and normal breast cells in the presence of different concentrations of Rutin-PEG-PtNP shows a concentration-dependent toxicity of the NPs in a way that even in minimal concentrations, they caused a decrease in the survival of cancer cells. Also, by comparing the survival of these two cell lines, it can be observed that the cancer cells have a much higher susceptibility to the NPs than normal cells. Also, cisplatin had a more potent anticancer effect than NPs on breast cancer cells. Furthermore, the NPs showed a time and dose-dependent toxicity on the breast cancer cells. Previous findings showed that PtNPs can have different degrees of toxicity on various cancer cell lines. It has been reported that PtNPs, in their pure or coated forms, can enter the cells through endocytic vesicles and exert toxic effects through the overproduction of ROS, damage to DNA, and inhibiting cell proliferation (Pedone et al., 2017). The DNA damage and apoptogenic properties of the PtNPs seem to be associated with the release of Pt^{2+} that can directly interact with DNA molecules leading to DNA strand breakage (Gehrke et al., 2011). Furthermore, intracellular cytotoxicity of PtNPs coated with biocompatible compounds has been reported to be related to the release of Pt^{2+} ions in the acidic lysosomal environment. In other words, although coating PtNPs with PEG can reduce their toxicity in the extracellular environment, upon entry to cancer cells, the cytotoxic potential of the particles can be recovered by the release of Pt^{2+} ions that leads to DNA damage and terminating cell proliferation (Pedone et al., 2017).

Cell viability and membrane integrity are considered important cytotoxicity markers in cytology studies. Our results showed that

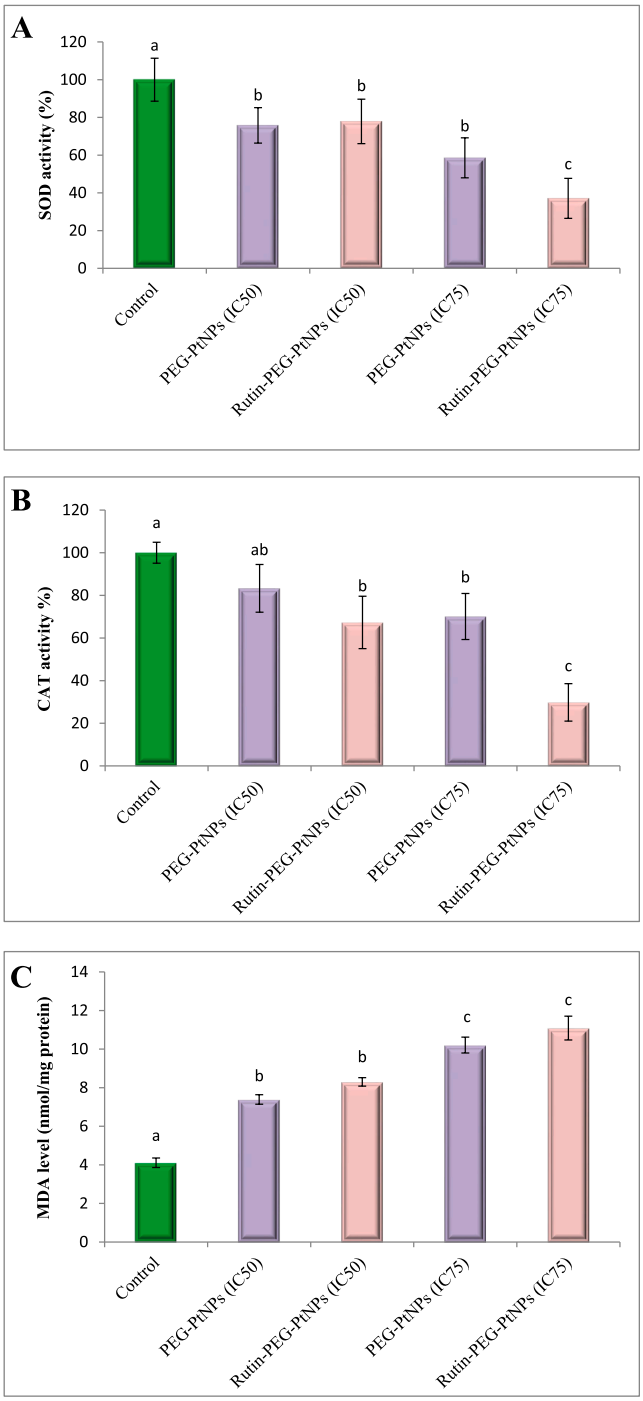

Fig. 7. Study of the oxidative stress biomarkers in NP-treated cancer cells. (A) SOD activity, (B) CAT activity, and (C) MDA level. Different letters display significant differences ($p < 0.05$).

treating breast cancer cells with Rutin-PEG-PtNPs led to reduced cell viability and increased membrane damage compared with the cells treated with PEG-PtNPs, which indicates the increasing toxicity effect of the NPs due to the presence of Rutin. Introducing a second material to PtNPs can improve their toxic performance through enhanced internalization, improved cancer cell targeting, or activation of additional cytotoxic mechanisms (Pedone et al., 2017). Several cytotoxic mechanisms, including DNA damage, generation of oxidative stress, cell cycle arrest, endoplasmic reticulum (ER) stress, and triggering apoptotic pathways have been reported in Rutin-treated cells (Guon and Chung, 2016; Panat et al., 2016; Hasani et al., 2018; Imani et al., 2021).

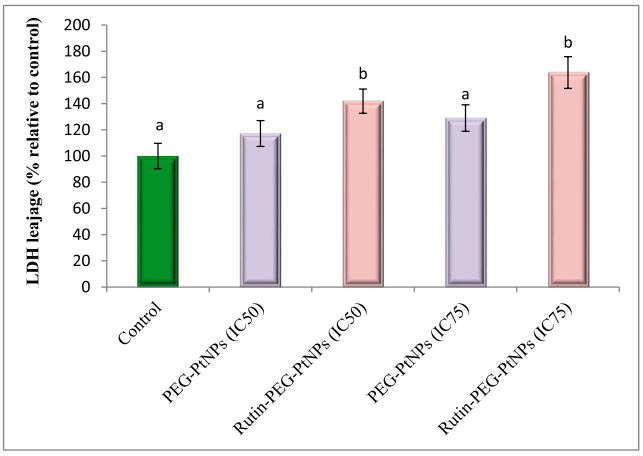

Fig. 8. LDH release from NP-treated cells, relative to control. Different letters display significant differences ($p < 0.05$).

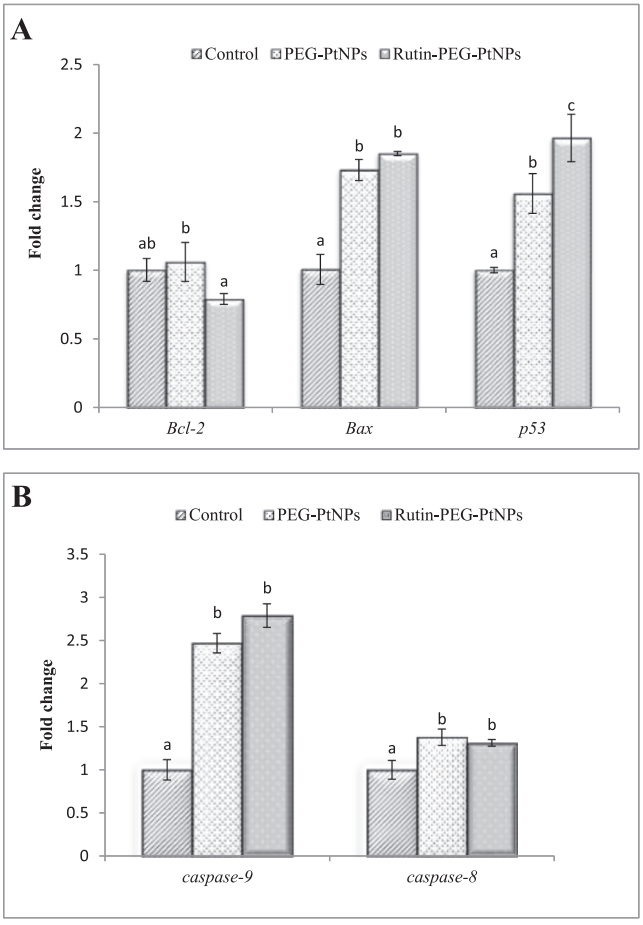

Fig. 9. Effect of Rutin-PEG-PtNPs on the expression of A) pro- and anti-apoptotic and B) caspase genes in MCF-7 cells. A significant increase in the expression of the genes associated with apoptosis was noticed. Different letters display significant differences ($p < 0.05$).

Therefore, following the exposure of cancer cells to Rutin-PEG-PtNPs, several toxic pathways associated with Rutin and PtNPs are simultaneously activated, which inhibit cell proliferation and induce cell death.

Comparing the cytotoxic effect of Rutin-PEG-PtNPs on breast cancer cells and normal breast cells showed that the NPs were more toxic for the cancer cells. Two important factors, including high metabolic activity

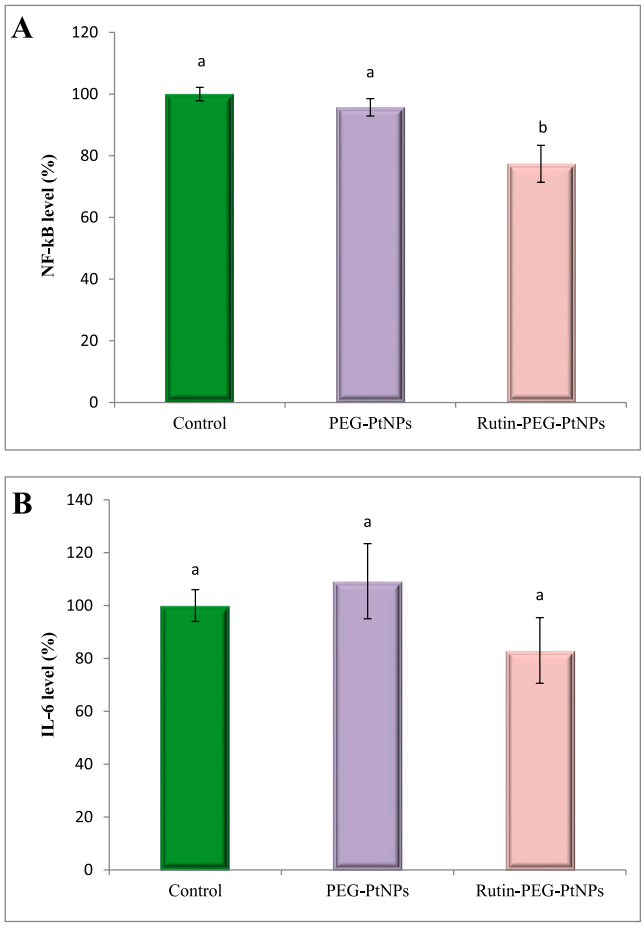

Fig. 10. Effect of PEG-PtNPs and Rutin-PEG-PtNPs on A) NF-κB and B) IL-6 level in supernatant from MCF-7 cell culture. Rutin-PEG-PtNPs caused an increase in the level of both cytokines. Different letters show significant differences ($p < 0.05$).

and mitochondrial membrane dysfunction, can be considered as the main reasons for the higher susceptibility of cancer cells to the synthesized NPs. Generally, due to the higher metabolic activity along with mitochondrial dysfunction, the level of ROS typically increases in cancer cells in comparison with the normal cells, which makes them more susceptible to oxidative stress (Navaneetha-Krishnan et al., 2019). Therefore, further generation of ROS molecules by the synthesized NPs will probably cause cancer cells to reach the oxidative stress threshold sooner than normal cells, which can subsequently lead to cell death.

Furthermore, as described above, endocytic vesicles are known as the most important diffusion route of PtNPs into a cell. Due to the high metabolic rate of cancer cells, the entry of extracellular compounds into these cells is accelerated. Therefore, the entrance of the synthesized NPs into cancer cells is faster than normal cells, which can explain their high toxicity effects on cancer cells. Previous studies reported apoptosis induction and cell cycle inhibition in various Rutin-treated cancer cell lines (Chen et al., 2013; Pedone et al., 2017). Chen et al., (2013) found that Rutin can induce G2/M arrest in the cell cycle progression and induce cell apoptosis. Furthermore, they associated apoptosis induction with a decreased *Bcl-2* expression and decreased Bcl-2/Bax ratio in Rutin-treated cells. In another study, Alshatwi et al., (2015) found that treating human cervical cancer cells with PtNPs resulted in the cell cycle arrest at the G2/M phase in response to DNA damage. It was also observed that PtNPs induce apoptotic cell death of the U87 glioma cell line, through mitochondrial degradation, vacuole formation, and up-regulation of mediator *caspases* and *p53* gene levels (Kutwin et al., 2017). Shiny et al., (2016) contributed anticancer properties of

biosynthesized PtNPs to DNA damage and mitochondria-mediated apoptosis in lung cancer cells. Furthermore, it was observed that PtNPs can induce genotoxicity and apoptotic activity in cancer cells via oxidative stress-mediated *Bax/Bcl2* and *caspase* gene expression, which is in agreement with our data (Almarzoug et al., 2020). Therefore, the apoptogenic feature of Rutin-PEG-PtNPs, observed in our study can be associated with both Rutin and Pt particles.

Alteration of the expression of apoptosis-regulating genes in breast cancer cells that were exposed to Rutin-PEG-PtNPs showed that the NPs caused an increase in the expression of the *p53*, *Bax*, *Caspase-8*, and *Caspase-9* genes, and also an insignificant downregulation of the *Bcl-2* gene. The P53 protein is a tumor suppressor that is involved in the promotion of cell cycle arrest and apoptosis induction in response to unfavorable conditions and cell damage. The decision to induce cell cycle arrest or apoptosis is related to several factors, such as the P53 level, cellular context, and environment. It was suggested that in response to severe cell damage, especially DNA damage, apoptosis induction is the more dominant outcome driven by the P53 protein (Shen and White, 2001). In addition to the regulation of the genes that are associated with cell cycle progression, studies suggest that the P53 mediates cell apoptosis by regulating the apoptosis-regulated genes, including the Bcl-2 family members (Shen and White, 2001). The Bcl-2 family proteins are divided into two categories, including proapoptotic proteins such as Bax and Bak, and antiapoptotic proteins such as the Bcl-2. Accumulative evidence suggests that the P53 mediates apoptosis through the upregulation of the proapoptotic genes and attenuation of the antiapoptotic ones (Aubrey et al., 2018). As observed in our study, treating the breast cancer cells with Rutin-PEG-PtNPs considerably upregulated the expression of the *p53* and *Bax* genes. Cell damage caused by the toxic effects of Rutin and Pt probably leads to the induction of *p53* expression, which, depending on the cell conditions, inhibits the cell cycle progression and/or induces apoptosis through the upregulation of the proapoptotic genes, including the *Bax* gene. The increased *Bax/Bcl-2* ratio is an important determinant favoring the progression of cell apoptosis. Therefore, the increased expression of the *Bax* and slight downregulation of the *Bcl-2* gene, which was observed in our work, suggest the apoptogenic outcomes caused by exposure to Rutin-PEG-PtNPs.

Caspase-8 and caspase-9 are representatives of the initiator caspases that are activated through stress signals such as DNA and mitochondrial membrane damage, which results in the activation of downstream effector caspases leading to cell death (Shen and White, 2001). It has been found that the activation of the P53 protein, and subsequently cytochrome *c* release from mitochondria leads to the activation of the caspase-9, which in turn activates downstream caspases, including caspases-2, −6, −7, −8, and −10, all in a caspase-9-dependent manner. The outcome of this event is the degradation of cell structural proteins and cell death during a process called intrinsic apoptosis (Slee et al., 1999). In contrast, Caspase-8 is an initiator caspase that is activated by death receptors such as tumor necrosis factor receptor 1 (TNFR1) and Fas which leads to the activation of downstream caspases and induction of the extrinsic apoptosis pathway (Tummers and Green, 2017). As noted above, treating breast cancer cells with Rutin-PEG-PtNPs caused a more intense upregulation of the *caspase-9* gene than the *caspase-8*. Considering the significant upregulation of the *p53*, *Bax*, and *caspase-9*, it could be concluded that the activation of the intrinsic apoptosis is likely a dominant outcome of treating breast cancer cells with Rutin-PEG-PtNPs.

Considering the oxidative stress biomarkers, including MDA level, and SOD and CAT activity, confirmed the generation of oxidative stress in NPs-treated cells. The reduced activity of the SOD, and CAT activity as well as the significant increase in MDA level in Rutin-PEG-PtNPS treated cells confirms that the NPs can generate high levels of ROS molecules which disrupt cellular redox balance. As a consequence, the induced oxidative stress can damage cell components, including DNA, mitochondria, and cytoplasmic membrane which leads to cell apoptosis and necrosis (Alarifi et al., 2014). Mitochondria are the predominant site of ROS generation and thus, oxidative stress damage could accumulate more extensively in mitochondria than in the rest of the cellular components (Zorov et al., 2014). The mitochondrial membrane damage can lead to cytochrom c release and initiate the intrinsic apoptosis pathway, which is in agreement with the results of gene expression assay.

NF-κB is a transcription factor involved with the development of breast tumors and the emergence of drug-resistant phenotype (Xia et al., 2018). The activation of NF-κB is also associated with the activation of several pro-inflammatory cytokines, including IL-6, which has a vital role in cancer progression (Abdel-Hakeem et al., 2021). Our results revealed that Rutin-PEG-PtNPs reduced NF-κB and IL-6 levels in breast cancer cells. Previous studies revealed that Rutin attenuates proinflammatory cytokine levels, including IL-6 through inhibition of the NF-κB, which is in agreement with our results (Sun et al., 2017; Youssef et al., 2022).

5. Conclusions

This work investigated the anticancer potential and mechanism of green synthesized PtNPs coated with PEG and conjugated with Rutin, for the first time and reported promising anticancer properties of the NPs. Rutin-PEG-PtNPs remarkably reduced the viability of breast cancer cells and had higher toxicity for cancer cells than normal breast cells. The cytotoxic effect of Rutin-PEG-PtNPs on breast cancer cells was time and dose-dependent, which altered the antioxidant defense mechanisms of cancer cells, causing cell damage. Considering the intense upregulation of the *p53*, *Bax*, and *caspase-9* gene, slight downregulation of the *Bcl-2* gene, as well as upregulation of the *caspase-8* gene, it could be concluded that Rutin-PEG-PtNPs likely exert cytotoxic effects on breast cancer cells through the activation of p53-mediated intrinsic apoptosis pathways. Our work indicates that Rutin-PEG-PtNPs can be regarded as a potent antiproliferative candidate against breast cancer cells and PEG-PtNPs can be considered as a platform for preparing novel anticancer drug formulations. The limitations of this research include the lack of *in-vivo* experiments and the limited number of studied cancer cell lines. In addition, more investigations are necessary to elucidate further the molecular anticancer mechanisms of Rutin-PEG-PtNPs.

Conflict of interest

None.

Declaration of competing interest

The authors declare that they have no known competing financial interests or personal relationships that could have appeared to influence the work reported in this paper.

Acknowledgements

This study was supported by Heilongjiang Science Foundation (Grant No.LC2018039), Wujieping Medical Foundation (Grant no. 320.6750.2020-20-27, and Wujieping Medical Foundation (Grant No. 320.6750.2023-11-10).

References

Abdel-Hakeem, M.A., Mongy, S., Hassan, B., Tantawi, O.I., Badawy, I., 2021. Curcumin loaded chitosan-protamine nanoparticles revealed antitumor activity via suppression of NF-κB, proinflammatory cytokines and Bcl-2 gene expression in the breast cancer cells. J. Pharm. Sci. 110 (9), 3298–3305. https://doi.org/10.1016/j.xphs.2021.06.004.

Ahamed, M., Akhtar, M.J., Siddiqui, M.A., Ahmad, J., Musarrat, J., Al-Khedhairy, A.A., AlSalhi, M.S., Alrokayan, S.A., 2011. Oxidative stress mediated apoptosis induced by nickel ferrite nanoparticles in cultured A549 cells. Toxicology 283 (2–3), 101–108. https://doi.org/10.1016/j.tox.2011.02.010.

Alarifi, S., Ali, D., Alkahtani, S., Alhader, M.S., 2014. Iron oxide nanoparticles induce oxidative stress, DNA damage, and caspase activation in the human breast cancer cell line. Biol. Trace. Elem. Rese. 159, 416–424. https://doi.org/10.1007/s12011-014-9972-0.

Almarzoug, M.H., Ali, D., Alarifi, S., Alkahtani, S., Alhadheq, A.M., 2020. Platinum nanoparticles induced genotoxicity and apoptotic activity in human normal and cancer hepatic cells via oxidative stress-mediated Bax/Bcl-2 and caspase-3 expression. Environ. Toxicol. 35 (9), 930–941. https://doi.org/10.1002/tox.22929.

Alshatwi, A.A., Athinarayanan, J., Vaiyapuri Subbarayan, P., 2015. Green synthesis of platinum nanoparticles that induce cell death and G2/M-phase cell cycle arrest in human cervical cancer cells. J. Mater. Sci. Mater. Med. 26, 1–9. https://doi.org/10.1007/s10856-014-5330-1.

Aubrey, B.J., Kelly, G.L., Janic, A., Herold, M.J., Strasser, A., 2018. How does p53 induce apoptosis and how does this relate to p53-mediated tumour suppression? Cell. Death. Differ. 25 (1), 104–113. https://doi.org/10.1038/cdd.2017.169.

Aygun, A., Gülbagca, F., Ozer, L.Y., Ustaoglu, B., Altunoglu, Y.C., Baloglu, M.C., Atalar, M.N., Alma, M.H., Sen, F., 2020. Biogenic platinum nanoparticles using black cumin seed and their potential usage as antimicrobial and anticancer agent. J. Pharm. Biomed. Anal. 179, 112961 https://doi.org/10.1016/j.jpba.2019.112961.

Banafa, A.M., Roshan, S., Liu, Y.Y., Chen, H.J., Chen, M.J., Yang, G.X., He, G.Y., 2013. Fucoidan induces G 1 phase arrest and apoptosis through caspases-dependent pathway and ROS induction in human breast cancer MCF-7 cells. J. Huazhong. Uni. Sci. Technol. [Med. Sci.] 33, 717–724. https://doi.org/10.1007/s11596-013-1186-8.

Chen, H., Miao, Q., Geng, M., Liu, J., Hu, Y., Tian, L., Pan, J., Yang, Y., 2013. Anti-tumor effect of rutin on human neuroblastoma cell lines through inducing G2/M cell cycle arrest and promoting apoptosis. Sci. World. J. 2013 https://doi.org/10.1155/2013/269165.

Farasat, M., Niazvand, F., Khorsandi, L., 2020. Zinc oxide nanoparticles induce necroptosis and inhibit autophagy in MCF-7 human breast cancer cells. Biologia 75, 161–174. https://doi.org/10.2478/s11756-019-00325-9.

Gehrke, H., Pelka, J., Hartinger, C.G., Blank, H., Bleimund, F., Schneider, R., Gerthsen, D., Bräse, S., Crone, M., Türk, M., Marko, D., 2011. Platinum nanoparticles and their cellular uptake and DNA platination at non-cytotoxic concentrations. Arch. Toxicol. 85, 799–812. https://doi.org/10.1007/s00204-010-0636-3.

Guon, T.E., Chung, H.S., 2016. Hyperoside and rutin of Nelumbo nucifera induce mitochondrial apoptosis through a caspase-dependent mechanism in HT-29 human colon cancer cells. Oncol. Lett. 11 (4), 2463–2470. https://doi.org/10.3892/ol.2016.4247.

Gurunathan, S., Jeyaraj, M., Kang, M.H., Kim, J.H., 2019. Tangeretin-assisted platinum nanoparticles enhance the apoptotic properties of doxorubicin: combination therapy for osteosarcoma treatment. Nanomater. 9 (8), 1089. https://doi.org/10.3390/nano9081089.

Hasani, N.A.H., Amin, I.M., Kamaludin, R., Rosdyd, N.M.M.N.M., Ibahim, M.J., Kadir, S. H.S.A., 2018. P53 and Cyclin B1 Mediate Apoptotic Effects of Apigenin AND Rutin in ERi+-Breast Cancer MCF-7 Cells. J. Teknol. 80 (1).

Imani, A., Maleki, N., Bohlouli, S., Kouhsoltani, M., Sharifi, S., Maleki Dizaj, S., 2021. Molecular mechanisms of anticancer effect of rutin. Phytother. Res. 35 (5), 2500–2513. https://doi.org/10.1002/ptr.6977.

Khursheed, R., Dua, K., Vishwas, S., Gulati, M., Jha, N.K., Aldhafeeri, G.M., Alanazi, F.G., Goh, B.H., Gupta, G., Paudel, K.R., Hansbro, P.M., 2022. Biomedical applications of metallic nanoparticles in cancer: Current status and future perspectives. Biomed. Pharmacother. 150, 112951 https://doi.org/10.1016/j.biopha.2022.112951.

Kızılbey, K., 2019. Optimization of rutin-loaded PLGA nanoparticles synthesized by single-emulsion solvent evaporation method. Acs Omeg. 4 (1), 555–562. https://doi.org/10.1021/acsomega.8b02767.

Kutwin, M., Sawosz, E., Jaworski, S., Hinzmann, M., Wierzbicki, M., Hotowy, A., Grodzik, M., Winnicka, A., Chwalibog, A., 2017. Investigation of platinum nanoparticle properties against U87 glioblastoma multiforme. Arch. Med. Sci. 13 (6), 1322–1334.

Livak, K.J., Schmittgen, T.D., 2001. Analysis of relative gene expression data using real-time quantitative PCR and the 2− ΔΔCT method. Methods 25 (4), 402–408. https://doi.org/10.1006/meth.2001.1262.

Muddineti, O.S., Ghosh, B., Biswas, S., 2015. Current trends in using polymer coated gold nanoparticles for cancer therapy. Int. J. Pharm. 484 (1–2), 252–267. https://doi.org/10.1016/j.ijpharm.2015.02.038.

Mukherjee, S., Kotcherlakota, R., Haque, S., Bhattacharya, D., Kumar, J.M., Chakravarty, S., Patra, C.R., 2020. Improved delivery of doxorubicin using rationally designed PEGylated platinum nanoparticles for the treatment of melanoma. Mater. Sci. Eng. C 108, 110375. https://doi.org/10.1016/j.msec.2019.110375.

NavaneethaKrishnan, S., Rosales, J.L., Lee, K.Y., 2019. ROS-mediated cancer cell killing through dietary phytochemicals. Oxid. Med. Cell. Longev. 2019 https://doi.org/10.1155/2019/9051542.

Panat, N.A., Singh, B.G., Maurya, D.K., Sandur, S.K., Ghaskadbi, S.S., 2016. Troxerutin, a natural flavonoid binds to DNA minor groove and enhances cancer cell killing in response to radiation. Chem. Biol. Interact. 251, 34–44. https://doi.org/10.1016/j.cbi.2016.03.024.

Pawar, A.A., Sahoo, J., Verma, A., Lodh, A., Lakkakula, J., 2021. Usage of Platinum Nanoparticles for Anticancer Therapy over Last Decade: A Review. Part. Part. Syst. Charact. 38 (10), 2100115. https://doi.org/10.1002/ppsc.202100115.

Pedone, D., Moglianetti, M., De Luca, E., Bardi, G., Pompa, P.P., 2017. Platinum nanoparticles in nanobiomedicine. Chem. Soc. Rev. 46 (16), 4951–4975. https://doi.org/10.1039/C7CS00152E.

Phadatare, M.R., Khot, V.M., Salunkhe, A.B., Thorat, N.D., Pawar, S.H., 2012. Studies on polyethylene glycol coating on NiFe2O4 nanoparticles for biomedical applications. J. Magn. Magn. Mater. 324 (5), 770–772. https://doi.org/10.1016/j.jmmm.2011.09.020.

Ramaswamy, S., Dwarampudi, L.P., Kadiyala, M., Kuppuswamy, G., Reddy, K.V.V.S., Kumar, C.K.A., Paranjothy, M., 2017. Formulation and characterization of chitosan encapsulated phytoconstituents of curcumin and rutin nanoparticles. Int. J. Biol. Macromol. 104, 1807–1812. https://doi.org/10.1016/j.ijbiomac.2017.06.112.

Saha, S., Mishra, A., 2020. A facile preparation of rutin nanoparticles and its effects on controlled growth and morphology of calcium oxalate crystals. J. Cryst. Growth. 540, 125635 https://doi.org/10.1016/j.jcrysgro.2020.125635.

Shen, Y., and White, E., 2001. p53-dependent apoptosis pathways. https://doi.org/10.1016/S0065-230X(01)82002-9.

Shiny, P.J., Mukherjee, A., Chandrasekaran, N., 2016. DNA damage and mitochondria-mediated apoptosis of A549 lung carcinoma cells induced by biosynthesised silver and platinum nanoparticles. RSC. Adv. 6 (33), 27775–27787. https://doi.org/10.1039/C5RA27185A.

Slee, E.A., Harte, M.T., Kluck, R.M., Wolf, B.B., Casiano, C.A., Newmeyer, D.D., Wang, H. G., Reed, J.C., Nicholson, D.W., Alnemri, E.S., Green, D.R., 1999. Ordering the cytochrome c–initiated caspase cascade: hierarchical activation of caspases-2,-3,-6,-7,-8, and-10 in a caspase-9–dependent manner. J. Cell. Biol. 144 (2), 281–292. https://doi.org/10.1083/jcb.144.2.281.

Sun, C.L., Wei, J., Bi, L.Q., 2017. Rutin attenuates oxidative stress and proinflammatory cytokine level in adjuvant induced rheumatoid arthritis via inhibition of NF-κB. Pharmacol. 100 (1–2), 40–49. https://doi.org/10.1159/000451027.

Sung, H., Ferlay, J., Siegel, R.L., Laversanne, M., Soerjomataram, I., Jemal, A., Bray, F., 2021. Global cancer statistics 2020: GLOBOCAN estimates of incidence and mortality worldwide for 36 cancers in 185 countries. CA: Cancer J Clin. 71 (3), 209–249. https://doi.org/10.3322/caac.21660.

Sur, S., Rathore, A., Dave, V., Reddy, K.R., Chouhan, R.S., Sadhu, V., 2019. Recent developments in functionalized polymer nanoparticles for efficient drug delivery system. Nano. Struct. Nano. Object. 20, 100397 https://doi.org/10.1016/j.nanoso.2019.100397.

Tummers, B., Green, D.R., 2017. Caspase 8: regulating life and death. Immunol Rev. 277 (1), 76–89. https://doi.org/10.1111/imr.12541.

Xia, L., Tan, S., Zhou, Y., Lin, J., Wang, H., Oyang, L., Tian, Y., Liu, L., Su, M., Wang, H., Cao, D., 2018. Role of the NFκB-signaling pathway in cancer. Onco. Target. Ther. 2063–2073 https://doi.org/10.2147/OTT.S161109.

Youssef, S.S., Ibrahim, N.K., El-Sonbaty, S.M., and El-Din Ezz, M.K., 2022. Rutin Suppresses DMBA Carcinogenesis in the Breast Through Modulating IL-6/NF-κB, SRC1/HSP90 and ER-α. Nat. Prod. Commun. 17(9), 1934578X221118213. https://doi.org/10.1177/1934578X221118213.

Zhang, C., Xu, C., Gao, X., Yao, Q., 2022. Platinum-based drugs for cancer therapy and anti-tumor strategies. Theranostics 12 (5), 2115. https://doi.org/10.7150/thno.69424.

Zhao, W., Li, J., Zhong, C., Zhang, X., Bao, Y., 2021. Green synthesis of gold nanoparticles from Dendrobium officinale and its anticancer effect on liver cancer. Drug. Deliv. 28 (1), 985–994. https://doi.org/10.1080/10717544.2021.1921079.

Zheng, B., Kong, T., Jing, X., Odoom-Wubah, T., Li, X., Sun, D., Lu, F., Zheng, Y., Huang, J., Li, Q., 2013. Plant-mediated synthesis of platinum nanoparticles and its bioreductive mechanism. J. Colloid. Interface. Sci. 396, 138–145. https://doi.org/10.1016/j.jcis.2013.01.021.

Zhou, Z., Fan, T., Yan, Y., Zhang, S., Zhou, Y., Deng, H., Cai, X., Xiao, J., Song, D., Zhang, Q., Cheng, Y., 2019. One stone with two birds: Phytic acid-capped platinum nanoparticles for targeted combination therapy of bone tumors. Biomater. 194, 130–138.

Zorov, D.B., Juhaszova, M., Sollott, S.J., 2014. Mitochondrial reactive oxygen species (ROS) and ROS-induced ROS release. Physiol. Rev. 94 (3), 909–950. https://doi.org/10.1152/physrev.00026.2013.